nature chemistry

ARTICLES

PUBLISHED ONLINE: 4 JULY 2016 | DOI: 10.1038/NCHEM.2552

Force-induced tautomerization in a single molecule

Janina N. Ladenthin[1], Thomas Frederiksen[2,3], Mats Persson[4], John C. Sharp[4], Sylwester Gawinkowski[5], Jacek Waluk[5,6] and Takashi Kumagai[1]*

Heat transfer, electrical potential and light energy are common ways to activate chemical reactions. Applied force is another way, but dedicated studies for such a mechanical activation are limited, and this activation is poorly understood at the single-molecule level. Here, we report force-induced tautomerization in a single porphycene molecule on a Cu(110) surface at 5 K, which is studied by scanning probe microscopy and density functional theory calculations. Force spectroscopy quantifies the force needed to trigger tautomerization with submolecular spatial resolution. The calculations show how the reaction pathway and barrier of tautomerization are modified in the presence of a copper tip and reveal the atomistic origin of the process. Moreover, we demonstrate that a chemically inert tip whose apex is terminated by a xenon atom cannot induce the reaction because of a weak interaction with porphycene and a strong relaxation of xenon on the tip as contact to the molecule is formed.

The mechanical activation and processing of molecules define the area of 'mechanochemistry'[1] and are also involved in many important biological functions such as the senses of touch, hearing and balance[2]. Furthermore, mechanochemical reactions have been applied to mechanoresponsive materials[3] and play a crucial role in molecular machines such as molecular motors and enzymes[4–6]. Mechanochemical processes have been investigated on the macroscopic scale, where the spectroscopic signal results from an ensemble of a large number of molecules. For instance, the selective dissociation or bimolecular reactions of polymers and the co-crystallization behaviour of organic (pharmaceutical) compounds under mechanical force have been monitored using mass spectrometry[7], electron spin resonance spectroscopy[8], vibrational spectroscopy[9] and X-ray diffraction[10]. However, the detailed mechanisms behind mechanochemical processes remain poorly understood at the molecular level. Force-induced breaking and formation of chemical bonds are the most elementary steps in a mechanochemical reaction, but these processes cannot be directly accessed at the single-molecule level using conventional methods. Ever since its invention, non-contact atomic force microscopy (nc-AFM) has been used not only for imaging nanostructures on surfaces but also for characterizing chemical interactions on an atomic scale. In particular, nc-AFM operated under ultrahigh-vacuum conditions has enabled the direct measurement of the force needed for moving an individual atom or molecule[11–15] and for the peeling of physisorbed polymers from a metal surface[16]. Scanning tunnelling microscopy (STM) has also been used to study the mechanical breaking of NaCl films[17]. However, a force-induced bond rearrangement in a single molecule has not yet been reported.

The most common form of tautomerization, which is an important reaction in organic chemistry, involves the migration of hydrogen atoms via chemical bond breaking and formation. This process is a fruitful model of chemical reactions and is also related to several important chemical and biological processes, such as chromism[18] or enzymatic reactions[19]. Tautomerization is also attracting increasing attention in the field of nanoscience and technology because of its potential applications as a single-molecule switch, which is an essential component in single-molecule-based devices[20]. Accordingly, the tautomerization of adsorbed naphthalocyanine[21], tetraphenylporphyrin[22] and porphycene[23–26] molecules has been investigated using low-temperature STM. These experiments demonstrated switching of a single molecule either by inelastically tunnelling electrons or by thermal activation. For device applications, the mechanical sensitivity and stability of molecular switches are also crucial properties, but studies of these properties remain scarce.

An intriguing model system to study tautomerization is provided by the porphycene molecule. This molecule is a structural isomer of free-base porphyrin[27] and exhibits similar chemical properties. However, unlike porphyrin, porphycene has strong hydrogen bonds in the molecular cavity (the N–H···N moiety)[28], resulting in a much faster tautomerization rate[29]. The porphycene molecule has three different twofold degenerate tautomers defined by the position of the inner hydrogen atoms (Supplementary Fig. 1). Our previous studies have revealed that the relative stabilities of these different tautomers depend on the atomic structure of a Cu substrate and are largely determined by the interaction between the lone pairs of the imine (non-hydrogenated) N atoms and the surface atoms[24,25]. On Cu(110) the *cis*(−1) configuration is the most stable; STM images of a single molecule are shown in Fig. 1a,b. It has been demonstrated that reversible *cis*↔*cis* tautomerization (Fig. 1c) can be induced either by thermal activation or by the inelastic electron tunnelling process of an STM[23].

Here, we present tip-induced tautomerization of a single porphycene molecule studied by a combination of scanning probe microscopy and density functional theory (DFT). We find that the *cis* ↔ *cis* tautomerization can also be triggered merely by bringing the tip close to a molecule at zero bias voltage and at 5 K. Note that tautomerization by inelastically tunnelling electrons does not take place below a threshold voltage of ~150 mV, and the thermally induced process requires a temperature above ~80 K (ref. 23). Our combined experimental and theoretical study demonstrates that an external force (interaction) applied to a molecule by a metallic tip induces tautomerization.

[1]Department of Physical Chemistry, Fritz-Haber Institute of the Max-Planck Society, Faradayweg 4-6, 14195 Berlin, Germany. [2]Donostia International Physics Center (DIPC) – UPV/EHU, E-20018, San Sebastián, Spain. [3]IKERBASQUE, Basque Foundation for Science, E-48013, Bilbao, Spain. [4]Surface Science Research Centre and Department of Chemistry, University of Liverpool, Liverpool L69 3BX, UK. [5]Institute of Physical Chemistry, Polish Academy of Sciences, Kasprzaka 44/52, Warsaw 01-224, Poland. [6]Faculty of Mathematics and Natural Sciences, College of Science, Cardinal Stefan Wyszyński University, Dewajtis 5, 01-815 Warsaw, Poland. *e-mail: kuma@fhi-berlin.mpg.de

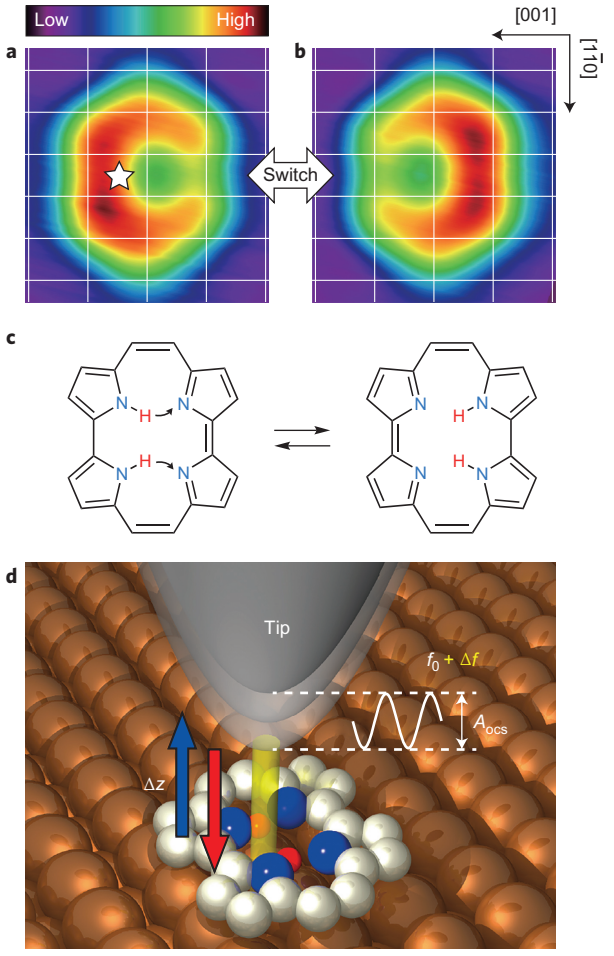

Figure 1 | Porphycene molecule on Cu(110) and schematic of the measurement configuration. a,**b**, STM images of a single porphycene molecule at 5 K (gap conditions: V_{bias} = –100 mV, I_t = 10 nA, size = 1.49 × 1.42 nm^2). The white grid represents the surface lattice of Cu(110). The white star indicates the lateral tip position during force spectroscopy in Fig. 2a–c. **c**, Molecular structure of *cis* porphycene, which can be reversibly switched between the two mirror reflected configurations. Curved arrows depict hydrogen transfer during tautomerization. **d**, Schematic of the tip-induced tautomerization experiment. The tip mounted on a tuning fork sensor oscillates at a resonance frequency f_0 of ~23 kHz with amplitude A_{ocs} of a few ångstroms. The frequency shift Δf caused by the interaction (yellow column) between the tip apex and molecule (or surface) is recorded while moving the tip down and up (Δz).

The nature of the tip-induced tautomerization was investigated using force spectroscopy of nc-AFM in the qPlus configuration[30], which enabled STM and nc-AFM measurements at the same time (see Supplementary Fig. 2 for simultaneously recorded STM and AFM images of porphycene). Figure 1d illustrates the experimental configuration. A tungsten tip mounted on a tuning fork sensor was oscillated at the resonance frequency f_0 and approached to and retracted from a molecule (Δz) while recording the frequency shift Δf. It was expected that the tip apex would be covered by Cu atoms, because it was gently crashed into the bare surface several times before measurement.

Figure 2a shows a typical $\Delta f(\Delta z)$ curve of a single cycle measurement over a molecule. The lateral tip position was fixed at the side of the pyrrole rings with the inner hydrogen atom attached, as indicated in Fig. 1a (the brighter side in the STM image). The $\Delta f(\Delta z)$ recorded over a molecule includes a long-range force from the Cu substrate that does not influence the tautomerization behaviour (Supplementary Fig. 3). Therefore, $\Delta f(\Delta z)$ measured over the bare Cu(110) surface was subtracted from the $\Delta f(\Delta z)$ measured over the molecule to eliminate its background component (Fig. 2a, inset)[31,32]. The background-subtracted force $F(\Delta z)$ and the tip–molecule interaction energy $U(\Delta z)$ were calculated from the background-subtracted $\Delta f(\Delta z)$ using the Sader–Jarvis method[33]. Figure 2b,c shows three typical $F(\Delta z)$ and $U(\Delta z)$ curves obtained under different tip conditions, as the apex was modified by applying a voltage pulse and/or by a controlled indentation of the tip into the bare surface. Note that $F(\Delta z)$ and $U(\Delta z)$ were highly reproducible as long as the tip conditions were identical (Supplementary Fig. 4). However, it was found that under certain tip conditions, $\Delta f(\Delta z)$ does not show a monotonic increase in the repulsive regime, which might be attributed to relaxation of the tip apex (Supplementary Fig. 5).

The tip-induced tautomerization event shows up as a discrete jump in $\Delta f(\Delta z)$ during the tip approach (Fig. 2a). STM images before and after each measurement (for example, in the inset of Fig. 2b) demonstrate that when this jump event occurs, the molecule switches from one *cis* configuration to the other mirror-reflected *cis* configuration without a change in the adsorption site. This tip-induced tautomerization is independent of a small bias voltage and tunnelling current (Supplementary Figs 6 and 7). In Fig. 2c, $U(\Delta z)$ shows that the attractive interaction increases after the jump (tautomerization) event. This is rationalized by a stronger attractive interaction of the tip apex with the imine N atoms of the 'acceptor' pyrrole than with the amine (hydrogenated) N atoms of the 'donor' pyrrole (Fig. 2h). As shown in the inset of Fig. 2c, the threshold potential (U_{th}) of tautomerization depends on the tip conditions and is distributed from –200 to –600 meV, and tautomerization occurs near the potential minimum (see also the distribution of the threshold distance in Supplementary Fig. 8).

In experiments, the *cis* → *cis* conversion was observed in most cases, and no *trans* molecule exists on Cu(110) after molecular deposition at room temperature. However, a stepwise tautomerization mechanism via the *trans* configuration is not ruled out, and rare instances of conversion to the *trans* configuration were indeed observed after the tip-induced tautomerization (Supplementary Fig. 9). This observation suggests that the *trans* configuration is a metastable state and that the *cis* → *cis* tautomerization may occur via the stepwise path, as discussed later. However, we were not able to conduct controlled experiments to stop the reaction at the *trans* configuration.

Tip-induced tautomerization depends strongly on the lateral tip position during its approach, as revealed by three-dimensional force mapping[34] over a molecule. Figure 2d–f presents cross-sectional maps of the background-subtracted $F(\Delta z)$ obtained with Tip 1 and along the [001] direction of Cu(110). The scan lines are indicated in Fig. 2g (see also Supplementary Fig. 10 for the position alignment of the force curves). The force maps clearly show that tautomerization can be exclusively induced when the tip is brought towards the donor pyrrole site. A very similar result was obtained under different tip conditions (see Supplementary Fig. 11 for the map measured with Tip 3).

The difference in $U(\Delta z)$ before and after tautomerization, $\Delta U(\Delta z) = U_{initial}(\Delta z) - U_{final}(\Delta z)$, represents the stability of the final *cis* state relative to the initial *cis* state in the presence of the tip, which is an important factor in the reaction. A positive $\Delta U(\Delta z)$ indicates that the final state is more stable than the initial one. Figure 2i,j shows $U(\Delta z)$ and $\Delta U(\Delta z)$ curves measured at three different lateral tip positions over the molecule (as indicated in Fig. 2g). At positions (i) and (ii), $\Delta U(\Delta z)$ turns from being negative to positive at short distances, but no such behaviour is observed at position (iii) and $\Delta U(\Delta z)$ increases monotonically with decreasing distance. This position dependence represents different energy gains of the system through the tip–molecule interaction.

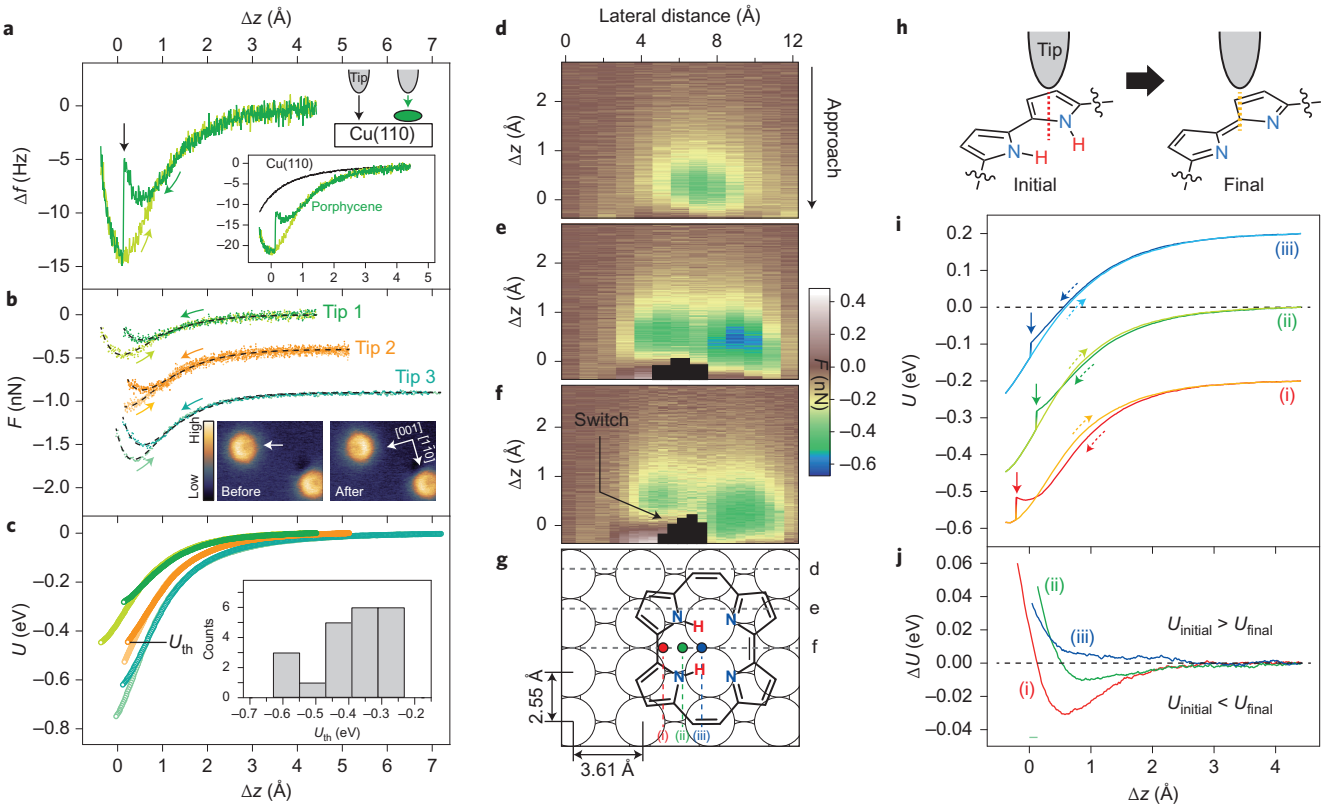

Figure 2 | Force spectroscopy of a single porphycene molecule. a, Background-subtracted $\Delta f(\Delta z)$ curves (green, approach; light green, retraction). Inset: $\Delta f(\Delta z)$ over a molecule (green) and the bare Cu(110) surface (black) before subtraction. The lateral tip position is indicated in Fig. 1a and V_{bias} was set to 0 V during the measurement. The initial tip height was fixed at a gap resistance of 10 GΩ (V_{bias} = 100 mV, I_t = 10 pA) over the bare Cu(110) surface and then laterally moved over a molecule with the feedback loop disabled. **b**, Background-subtracted $F(\Delta z)$ curves measured with three different tip conditions (labelled Tip 1 to Tip 3). The black dashed lines represent the fitted result to the Morse potential model $F_M = -E_d 2\kappa[e^{-\kappa(z-z_e)} - e^{-2\kappa(z-z_e)}]$, where E_d is the bond energy, κ the decay constant and z_e the equilibrium distance (fitting parameters are listed in Supplementary Table 1). Δz is the relative tip height with respect to z_e of each approach curve. For clarity, curves of Tip 2 and Tip 3 are offset vertically. Inset: STM images before and after measurement (the white arrow in the left image indicates the measured molecule). **c**, Background-subtracted $U(\Delta z)$ curves for the three different tips. Inset: Histogram of the threshold potential U_{th} collected from 21 different tip conditions. **d**–**f**, Background-subtracted $F(\Delta z)$ maps for approach measured along the [001] direction and obtained with Tip 1. The upper edge of the black area in **e** and **f** indicates the vertical tip position at which tautomerization takes place. **g**, Adsorption geometry of porphycene determined by DFT calculations. The black dashed lines represent the recorded lines of the force maps in **d**–**f**. **h**, Schematic of the initial and final states of tautomerization. **i**, Background-subtracted $U(\Delta z)$ curves measured at three different positions over a molecule indicated in **g** (obtained with Tip 1). For clarity, curves (i) and (iii) are offset vertically. **j**, ΔU ($= U_{initial} - U_{final}$) curves at the three different positions. Δz for **d**–**f** and **i**,**j** represents the relative tip height with respect to z_e of the approach curve at position (ii). Measurement parameters: (Tip 1) A_{ocs} = 1 Å, f_0 = 22,653 Hz, Q = 18,274; (Tip 2) A_{ocs} = 1 Å, f_0 = 22,645 Hz, Q = 33,855; (Tip 3) A_{ocs} = 1 Å, f_0 = 22,646 Hz, Q = 39,143.

A most interesting question is how the chemical reactivity of the tip apex affects a tip-induced reaction. For instance, a critical role of tip reactivity has been predicted by DFT calculations for AFM-induced Si atom hopping on Si(111)[35]. To examine the effects of tip reactivity, we functionalized the tip apex by adsorbing a single Xe atom using vertical manipulation[36] (Fig. 3a). This tip functionalization did not significantly influence the STM image (Fig. 3b,c), although the contrast is slightly enhanced compared to a normal metallic tip. However, the Xe tip dramatically changed the behaviour of $\Delta f(\Delta z)$ and tautomerization (Fig. 3d). Interestingly, no tautomerization can be induced, and $\Delta f(\Delta z)$ is non-monotonic in the repulsive potential regime. The $\Delta f(\Delta z)$ curves are identical in the approach and retraction of the tip. After the measurement, no change in the molecule was observed (Fig. 3b,c). Thus, we attribute the non-monotonic behaviour of $\Delta f(\Delta z)$ to a reversible relaxation of the Xe atom on the tip. The absence of tip-induced tautomerization in this case is not surprising in view of the magnitude of the interaction energy between the molecule and the Xe tip (Fig. 3e), which remains substantially smaller than for the metallic tip, as judged from the experimentally determined $U(\Delta z)$ (Fig. 2c).

Atomistic insights into the mechanism behind the tip-induced tautomerization can be gained by modelling the tip–molecule–surface system with DFT calculations. The supercell model used for this system is shown in Fig. 4a,b (see Methods and Supplementary Section 12 for details). The calculated background-subtracted $U(\Delta z)$ and $\Delta U(\Delta z)$ and the two-dimensional force map are shown in Fig. 4c–e (Supplementary Figs 12 and 13). Our calculations are able to reproduce quantitatively the key features of the experimental force map, $U(\Delta z)$ and $\Delta U(\Delta z)$ (Fig. 2f,i and j). The calculated attractive forces are smaller over the amine N atoms than over the imine N atoms (Fig. 4e) and the minimum in $\Delta U(\Delta z)$ becomes shallower when the tip approaches close to the centre of the molecule (Fig. 4d). The most notable differences are larger values for the tip–molecule interaction and the distinct potential minima over the rim at the donor pyrrole side (around Δx of −2 to −3 Å), which might be due to the idealized tip model with low-coordinated Cu atoms leading to the relatively reactive apex. It should also be noted that the uncertainty of the spring constant of the used qPlus sensor could cause a systematic error of 10–20% in the experimental $F(\Delta z)$ and $U(\Delta z)$ values[37].

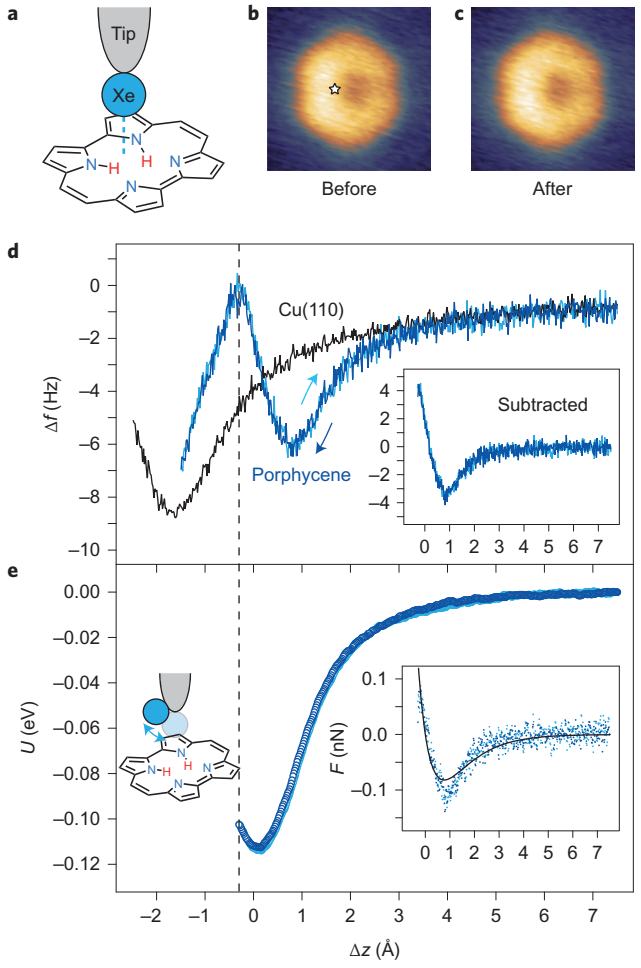

Figure 3 | Force spectroscopy of a single porphycene molecule with a Xe-terminated tip. a, Schematic of the experimental configuration. **b**,**c**, STM images with a Xe tip before (**b**) and after (**c**) the measurement (V_{bias} = 100 mV, I_t = 30 pA, 1.4 × 1.4 nm^2). The white star indicates the lateral tip position during the measurement. **d**, $\Delta f(\Delta z)$ curve measured over Cu(110) (black) and over porphycene (blue, approach; light blue, retraction). Inset: Background-subtracted $\Delta f(\Delta z)$. The subtraction is implemented in the regime before the second decrease of $\Delta f(\Delta z)$ takes place (indicated by the dashed line). **e**, Background-subtracted $U(\Delta z)$ curve. Inset: $F(\Delta z)$ curve. The solid line represents the best fitted result of the approach curve to the Morse potential model with parameters [E_d (eV), κ (Å^{-1})] = [0.114(±0.004), 0.98(±0.08)]. Δz is the relative tip height with respect to z_e. Measurement parameters: A_{ocs} = 1 Å, f_0 = 22,646 Hz, Q = 39,143.

A key question to understand the tip-induced tautomerization is how the reaction path (barrier) is influenced by the interaction with the tip. A first step in answering this question is to determine the reaction path in the absence of the tip. Our calculations of the minimum energy paths (MEPs) reveal that the tautomerization proceeds by a stepwise mechanism via one of two intermediate, degenerate *trans* configurations (Fig. 4f). The alternative concerted mechanism was found to have a significantly larger energy barrier (Supplementary Fig. 14). The barriers for the *cis* → *trans* and *trans* → *cis* conversions in the stepwise mechanism were calculated to be 203 and 19 meV, respectively, when including the zero-point energy (ZPE) corrections (Supplementary Section 14). The value for the first energy barrier is in good agreement with the experimentally determined thermal activation energy of ~170 meV, and the small value of the second barrier is consistent with the observation that the *trans* configuration is not detected in thermally or inelastically tunnelling electron-induced tautomerization, most probably because of its short lifetime (that is, the time resolution of STM, a few hundred microseconds, is not enough to capture it).

In the gas phase, the tautomerization barrier of porphycene is rather small (~70 meV)[38] and this reaction occurs very rapidly by quantum tunnelling[29]. It has also been found that the reaction barrier is essentially associated with the hydrogen bond strength (geometry) of the N-H···N moiety in the molecular cavity[39]. The increased barrier for the adsorbed porphycene on Cu(110) could be attributed to the change in the hydrogen bond through the formation of a dative bond of the lone pair orbitals of the imine N atoms with the surface Cu atoms. According to our calculations, this dative bonding is manifested by a slight distortion of the molecular frame from its planar geometry in the gas phase and consequently the donor pyrroles (amine nitrogen atoms) are slightly farther from the surface compared with the acceptor pyrroles (imine N atoms) (Fig. 4a). This bonding also causes lateral displacement of the molecule along the [001] axis by about 0.4 Å during tautomerization.

Our calculations further predict that the bonding geometry of the molecular cavity is also modified by the tip. The calculated N–H bond length as a function of tip height Δz and lateral position Δx (Fig. 4g) shows that the bond becomes elongated when the tip approaches the 'donor' pyrrole. Interestingly, this elongation already occurs in the attractive potential regime. In addition, a redshift of the N–H stretching energy was observed upon tip approach in single-molecule vibration spectroscopy with an STM, and this trend was also reproduced by our calculations (Supplementary Fig. 15). These results indicate a weakening of the N–H bond and a strengthening of the hydrogen bond in the molecular cavity, which is very consistent with a lowering of the tautomerization barrier upon tip approach. Moreover, our calculations of the MEP for stepwise tautomerization in the presence of a tip demonstrate that the overall barrier is indeed reduced when in close proximity (Fig. 4h). The reaction primarily correlates with the barrier height and the total energy difference ΔU between the initial and final states upon tip approach. As shown in Fig. 4h, at a relative tip displacement of $\Delta z = 0.20$ Å and $\Delta x = -1.8$ Å, the final *cis* configuration is slightly less stable than the initial *cis* configuration ($\Delta U = -60$ meV). Additionally, the MEP is substantially affected and the ZPE corrected barrier of 245 meV is even larger than the barrier in the absence of the tip. On even further approach ($\Delta z < 0$ Å), the final *cis* configuration becomes more stable than the initial *cis* configuration ($\Delta U = 59$ meV at $\Delta z = -0.05$ Å) and the barriers are reduced. The *trans* → *cis* barrier essentially vanishes at $\Delta z \leq -0.30$ Å and the *cis* → *trans* barrier is reduced to only 66 and 35 meV at $\Delta z = -0.30$ and -0.55 Å, respectively. Thus, at these short distances a small barrier may remain for the first *cis*→*trans* conversion, but the reaction could proceed via quantum tunnelling[40,41].

Finally, our calculations also rationalize the observed behaviour with a Xe-terminated tip. The calculated $U(\Delta z)$ was found to be significantly smaller than that of a Cu tip, and the simulation also predicted large geometric relaxations of the Xe atom on the tip when approaching the porphycene molecule (Supplementary Fig. 16). Furthermore, the calculated MEP in the presence of a Xe tip shows a significant increase in the overall energy barrier (Supplementary Fig. 17), which is consistent with the absence of tip-induced tautomerization. These results indicate the significance not only of the reactivity but also of the stiffness of the apex in the tip-induced reaction.

We have demonstrated that a combination of scanning probe experiments and DFT calculations opens a unique capability for studies of mechanochemistry at the single-molecule level. Moreover, the studied tip-induced reaction involving the reduction of the effective activation barrier invokes a catalytic process. In the present case, the reaction pathway is modified by bringing the tip (active site) to a molecule. In STM, controlled termination of the tip apex with

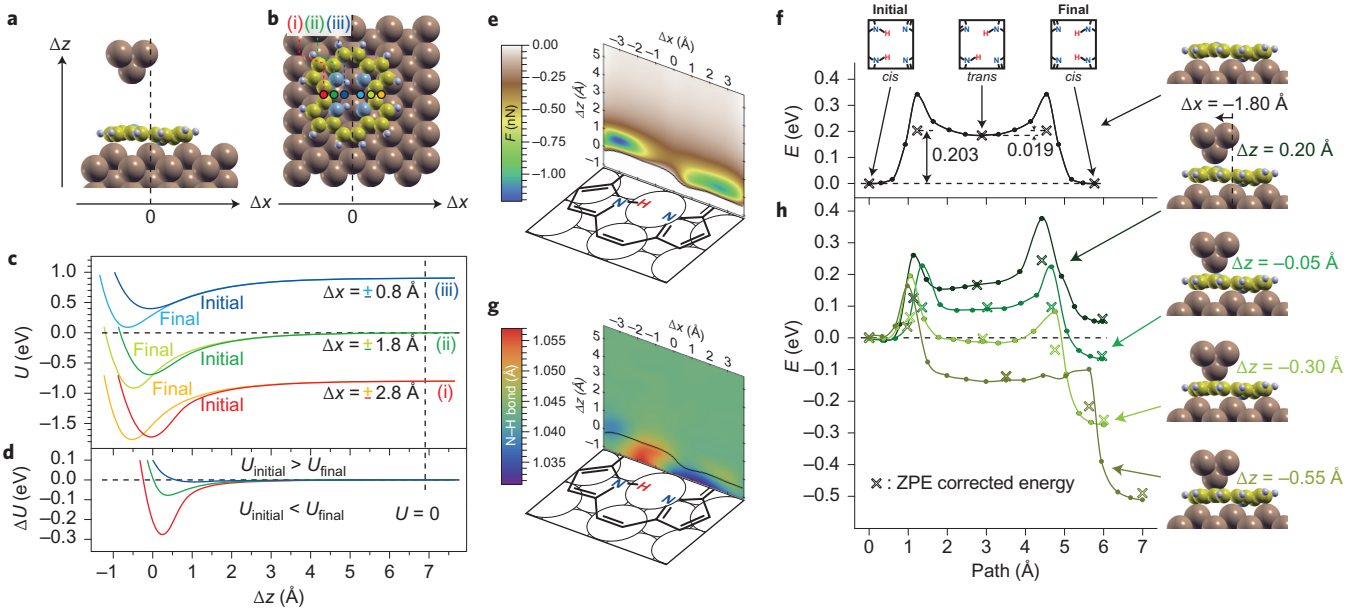

Figure 4 | Calculated force curves and MEPs for the tip–porphycene–surface system. a,**b**, Optimized structure and modelled Cu tip. **c**,**d**, Simulated background-subtracted $U(\Delta z)$ and $\Delta U(\Delta z)$ curves. The lateral tip position is indicated by the coloured dots in **b**. 'Initial' and 'Final' represent the curves over the donor and acceptor pyrroles, respectively (that is, corresponding to the curves before and after tautomerization). Δz is defined with respect to the potential minimum of the 'Initial' curve at position (ii). The curves for positions (i) and (iii) in **c** are offset vertically for clarity. **e**, Simulated two-dimensional force map over a molecule (only the $F < 0$ regime is shown). **f**, MEP for the *cis* → *cis* tautomerization of the adsorbed porphycene on Cu(110) determined by the nudged elastic band method. **g**, Two-dimensional plot of the N–H bond length as a function of tip position. The black line indicates the $F = 0$ contour. **h**, MEPs in the presence of the tip. The corresponding geometry is displayed on the right. Crosses in **f** and **h** represent ZPE corrected energies. The path length was obtained from the Euclidean distance between the images in configuration space.

various atoms and molecules is a well-established technique[42,43]. A systematic study using such chemically modified tips could also provide a novel insight into a catalytic reaction and lead to control of the reaction pathway and products at the atomic level.

Methods

Experiments were carried out in ultrahigh-vacuum conditions ($<2 \times 10^{-10}$ mbar). STM and nc-AFM measurements were performed at 5 K with a modified low-temperature STM/AFM (Omicron Nanotechnology) operated by a Nanonis Control System (Specs). Tuning fork sensors in the qPlus configuration were used with an electrochemically etched W tip (resonance frequency ~23 kHz, spring constant ~1,800 N m^{-1}, quality factor Q ~20,000–50,000 at 5 K). The bias voltage V_{bias} is applied to the sample. To minimize crosstalk between the STM and AFM channels, the tunnelling current was collected from the sample[44]. A single-crystalline Cu(110) was cleaned by repeated cycles of Ar ion sputtering and annealing. Porphycene molecules were evaporated from a Knudsen cell (at a temperature of ~450 K).

The tip–porphycene–copper surface system was modelled with periodic, plane-wave DFT calculations and a van der Waals density functional[45–47]. The Cu(110) surface was represented in a supercell by a four-layer slab with a 4×6 surface unit cell and a 20 Å vacuum region. The tip apex was modelled by a Cu_5 and $XeCu_5$ cluster with the relative coordinates of the Cu atoms fixed to those of the isolated cluster. The geometry and total energy of the combined system were determined by relaxing the molecule and the topmost two Cu layers for a range of tip positions and fixed supercell size. Background subtraction of the interaction energies was performed by also evaluating the total energy for supercells without the molecule. Reaction barriers were computed with the nudged elastic band method[48,49]. Further computational details are provided in Supplementary Section 12.

Received 10 September 2015; accepted 17 May 2016; published online 4 July 2016

References

1. Beyer, M. K. & Clausen-Schaumann, H. Mechanochemistry: the mechanical activation of covalent bonds. *Chem. Rev.* **105,** 2921–2948 (2005).
2. Gillespie, P. G. & Walker, R. G. Molecular basis of mechanosensory transduction. *Nature* **413,** 194–202 (2001).
3. Davis, D. A. *et al.* Force-induced activation of covalent bonds in mechanoresponsive polymeric materials. *Nature* **459,** 68–72 (2009).
4. Astumian, R. D. & Bier, M. Mechanochemical coupling of the motion of molecular motors to ATP hydrolysis. *Biophys. J.* **70,** 637–653 (1996).
5. Bustamante, C., Chemla, Y. R., Forde, N. R. & Izhaky, D. Mechanical processes in biochemistry. *Annu. Rev. Biochem.* **73,** 705–748 (2004).
6. Puchner, E. M. & Gaub, H. E. Single-molecule mechanoenzymatics. *Annu. Rev. Biophys.* **41,** 497–518 (2012).
7. Nguyen, T. Q. & Kausch, H. H. Effects of solvent viscosity on polystyrene degradation in transient elongational flow. *Macromolecules* **23,** 5137–5145 (1990).
8. Sohma, J. Mechanochemistry of polymers. *Prog. Polym. Sci.* **14,** 451–596 (1989).
9. Nguyen, K. L., Friščič, T., Day, G. M., Gladden, L. F. & Jones, W. Terahertz time-domain spectroscopy and the quantitative monitoring of mechanochemical cocrystal formation. *Nature Mater.* **6,** 206–209 (2007).
10. Halasz, I. *et al.* Real-time in situ powder X-ray diffraction monitoring of mechanochemical synthesis of pharmaceutical cocrystals. *Angew. Chem. Int. Ed.* **52,** 11538–11541 (2013).
11. Loppacher, Ch. *et al.* Direct determination of the energy required to operate a single molecule switch. *Phys. Rev. Lett.* **90,** 066107 (2003).
12. Ternes, M., Lutz, C. P., Hirjibehedin, C. F., Giessibl, F. J. & Heinrich, A. J. The force needed to move an atom on a surface. *Science* **319,** 1066–1069 (2008).
13. Sweetman, A. *et al.* Toggling bistable atoms via mechanical switching of bond angle. *Phys. Rev. Lett.* **106,** 136101 (2011).
14. Langewisch, G., Falter, J., Fuchs, H. & Schirmeisen, A. Forces during the controlled displacement of organic molecules. *Phys. Rev. Lett.* **110,** 036101 (2013).
15. Yamazaki, S. *et al.* Interplay between switching driven by the tunneling current and atomic force of a bistable four-atom Si quantum dot. *Nano Lett.* **15,** 4356–4363 (2015).
16. Kawai, S. *et al.* Quantifying the atomic-level mechanics of single long physisorbed molecular chains. *Proc. Natl Acad. Sci. USA* **111,** 3968–3972 (2014).
17. Bombis, Ch. *et al.* Mechanical behavior of nanocrystalline NaCl islands on Cu (111). *Phys. Rev. Lett.* **104,** 185502 (2010).
18. Ohshima, A., Momotake, A. & Arai, T. Photochromism, thermochromism, and solvatochromism of naphthalene-based analogues of salicylideneaniline in solution. *J. Photochem. Photobiol. A* **162,** 473–479 (2004).
19. Tapia, O., Andres, J. & Safont, V. S. Theoretical study of transition structures for intramolecular hydrogen transfer in molecular models representing D-ribulose 1,5-bisphosphate. A possible molecular mechanism for the enolization step in Rubisco. *J. Phys. Chem.* **98,** 4821–4830 (1994).
20. Heath, J. R. & Ratner, M. A. Molecular electronics. *Phys. Today* **56,** 43–49 (May 2003).

21. Liljeroth, P., Repp, J. & Meyer, G. Current-induced hydrogen tautomerization and conductance switching of naphthalocyanine molecules. *Science* **317,** 1203–1206 (2007).
22. Auwärter, W. *et al.* A surface-anchored molecular four-level conductance switch based on single proton transfer. *Nature Nanotech.* **7,** 41–46 (2012).
23. Kumagai, T. *et al.* Thermally and vibrationally induced tautomerization of single porphycene molecules on a Cu(110) surface. *Phys. Rev. Lett.* **111,** 246101 (2013).
24. Kumagai, T. *et al.* Controlling intramolecular hydrogen transfer in a porphycene molecule with single atoms or molecules located nearby. *Nature Chem.* **6,** 41–46 (2014).
25. Ladenthin, J. N. *et al.* Hot carrier-induced tautomerization within a single porphycene molecule on Cu(111). *ACS Nano* **9,** 7287–7295 (2015).
26. Kumagai, T. Direct observation and control of hydrogen-bond dynamics using low-temperature scanning tunneling microscopy. *Prog. Surf. Sci.* **90,** 239–291 (2015).
27. Vogel, E., Köcher, M., Schmickler, H. & Lex, J. Porphycene—a novel porphin isomer. *Angew. Chem. Int. Ed. Engl.* **25,** 257–259 (1986).
28. Gawinkowski, S. *et al.* Vibrations and hydrogen bonding in porphycene. *Phys. Chem. Chem. Phys.* **14,** 5489–5503 (2012).
29. Fita, P., Urbańska, N., Radzewicz, C. & Waluk, J. Ground- and excited-state tautomerization rates in porphycenes. *Chem. Eur. J.* **15,** 4851–4856 (2009).
30. Giessibl, F. J. Atomic resolution on Si(111)-(7×7) by noncontact atomic force microscopy with a force sensor based on a quartz tuning fork. *Appl. Phys. Lett.* **76,** 1470–1472 (2000).
31. Lantz, M. A. *et al.* Quantitative measurement of short-range chemical bonding forces. *Science* **291,** 2580–2583 (2001).
32. Ternes, M. *et al.* Interplay of conductance, force, and structural change in metallic point contacts. *Phys. Rev. Lett.* **106,** 016802 (2011).
33. Sader, J. E. & Jarvis, S. P. Accurate formulas for interaction force and energy in frequency modulation force spectroscopy. *Appl. Phys. Lett.* **84,** 1801–1803 (2004).
34. Mohn, F., Gross, L. & Meyer, G. Measuring the short-range force field above a single molecule with atomic resolution. *Appl. Phys. Lett.* **99,** 053106 (2011).
35. Sugimoto, Y. *et al.* Role of tip chemical reactivity on atom manipulation process in dynamic force microscopy. *ACS Nano* **7,** 7370–7376 (2013).
36. Eigler, D. M., Lutz, C. P. & Rudge, W. E. An atomic switch realized with the scanning tunnelling microscope. *Nature* **352,** 600–603 (1991).
37. Falter, J. *et al.* Calibration of quartz tuning fork spring constants for non-contact atomic force microscopy direct mechanical measurements and simulations. *Beilstein J. Nanotechnol.* **5,** 507–516 (2014).
38. Kozlowski, P. M., Zgierski, M. Z. & Baker, J. The inner-hydrogen migration and ground-state structure of porphycene. *J. Chem. Phys.* **109,** 5905–5913 (1998).
39. Ciąćka, P. *et al.* Tautomerism in porphycenes: analysis of rate-affecting factors. *J. Phys. Chem. B* **119,** 2292–2301 (2015).
40. Kumagai, T. *et al.* Direct observation of hydrogen-bond exchange within a single water dimer. *Phys. Rev. Lett.* **100,** 166101 (2008).
41. Meng, X. *et al.* Direct visualization of concerted proton tunnelling in a water nanocluster. *Nature Phys.* **11,** 235–239 (2015).
42. Gross, L., Mohn, F., Moll, N., Liljeroth, P. & Meyer, G. The chemical structure of a molecule resolved by atomic force microscopy. *Science* **325,** 1110–1114 (2009).
43. Mohn, F., Schuler, B., Gross, L. & Meyer, G. Different tips for high-resolution atomic force microscopy and scanning tunneling microscopy of single molecules. *Appl. Phys. Lett.* **102,** 073109 (2013).
44. Majzik, Z. *et al.* Simultaneous current, force and dissipation measurements on the Si(111) 7 × 7 surface with an optimized qPlus AFM/STM technique. *Beilstein J. Nanotechnol.* **3,** 249–259 (2012).
45. Dion, M., Rydberg, H., Schröder, E., Langreth, D. C. & Lundqvist, B. I. Van der Waals density functional for general geometries. *Phys. Rev. Lett.* **92,** 246401 (2004).
46. Román-Pérez, G. & Soler, J. M. Efficient implementation of a van der Waals density functional: application to double-wall carbon nanotubes. *Phys. Rev. Lett.* **103,** 096102 (2009).
47. Klimeš, J., Bowler, D. R. & Michaelides, A. Chemical accuracy for the van der Waals density functional. *J. Phys. Condens. Matter* **22,** 022201 (2010).
48. Mills, G., Jónsson, H. & Schenter, G. K. Reversible work transition state theory: application to dissociative adsorption of hydrogen. *Surf. Sci.* **324,** 305–337 (1995).
49. Henkelman, G., Uberuaga, B. P. & Jónsson, H. A climbing image nudged elastic band method for finding saddle points and minimum energy paths. *J. Chem. Phys.* **113,** 9901–9904 (2000).

Acknowledgements

J.N.L. and T.K. thank L. Grill, M. Wolf, A. Sweetman, O. Custance and A. Tkatchenko for discussions. T.K. acknowledges the support of the Morino Foundation for Molecular Science. T.F. acknowledges the support of the Basque Deptamento de Educación and the UPV/EHU (IT-756-13), the Spanish Ministerio de Economía y Competitividad (MAT2013-46593-C6-2-P) and the EU Integrated Project PAMS (610446). M.P. acknowledges computer time allocated on ARCHER through the Materials Chemistry Consortium funded by EPSRC grant no. EP/L000202, on Polaris through N8 HPC funded by EPSRC grant no. EP/K000225/1 and on Chadwick at the University of Liverpool. S.G. and J.W. acknowledge support from the Polish National Science Centre (grant no. DEC-2011/02/A/ST5/00043).

Author contributions

T.K. conceived the experiments. J.N.L. and T.K. performed the measurements and analysed data. T.F., M.P. and J.C.S. performed all the DFT calculations. S.G. and J.W. provided porphycene molecules. T.K. wrote the manuscript. All authors discussed the results and commented on the manuscript.

Additional information

Supplementary information is available in the online version of the paper. Reprints and permissions information is available online at www.nature.com/reprints. Correspondence and requests for materials should be addressed to T.K.

Competing financial interests

The authors declare no competing financial interests.

nature chemistry

SUPPLEMENTARY INFORMATION

DOI: 10.1038/NCHEM.2552

Force-induced tautomerization in a single molecule

Janina N. Ladenthin[1], Thomas Frederiksen[2,3], Mats Persson[4], John C. Sharp[4], Sylwester Gawinkowski[5], Jacek Waluk[5,6], Takashi Kumagai[1]*

[1]Department of Physical Chemistry, Fritz-Haber Institute of the Max-Planck Society, Faradayweg 4-6, 14195 Berlin, Germany.

[2]Donostia International Physics Center (DIPC) – UPV/EHU, E-20018, San Sebastián, Spain.

[3] IKERBASQUE, Basque Foundation for Science, E-48013, Bilbao, Spain.

[4]Surface Science Research Centre and Department of Chemistry, University of Liverpool, Liverpool L69 3BX, UK.

[5]Institute of Physical Chemistry, Polish Academy of Sciences, Kasprzaka 44/52, Warsaw 01-224, Poland.

[6]Faculty of Mathematics and Natural Sciences, College of Science, Cardinal Stefan Wyszyński University, Dewajtis 5, 01-815 Warsaw, Poland

*Correspondence to kuma@fhi-berlin.mpg.de

Table of contents

1. Tautomers of porphycene

Porphycene has three twofold-degenerate tautomers according to the position of the inner H atoms. In the *trans* configuration (**Fig. 1a**) the H atoms are located on the diagonal pyrrole rings, while they are located on the same side in the *cis*-1 (**Fig. 1b**) and *cis*-2 (**Fig. 1c**) configurations. In the gas phase, calculations have predicted that *trans* and *cis*-1 configurations have a comparable total energy (*trans* is slightly more favorable), but *cis*-2 is considerably unstable due to the steric hindrance[1]. However, the energetically preferred tautomer on a metal surface is significantly affected by the interaction between the molecule and the surface. Our previous studies have revealed that the *cis*-1 configuration becomes the most stable state on Cu(110) and molecules are exclusively found in the *cis*-1 configuration in experiment[2]. On the other hand, the *trans* configuration becomes the thermodynamically stable state on Cu(111), but *trans* molecules can be converted to the meta-stable *cis*-1 configuration via an inelastic electron tunneling process in STM[3].

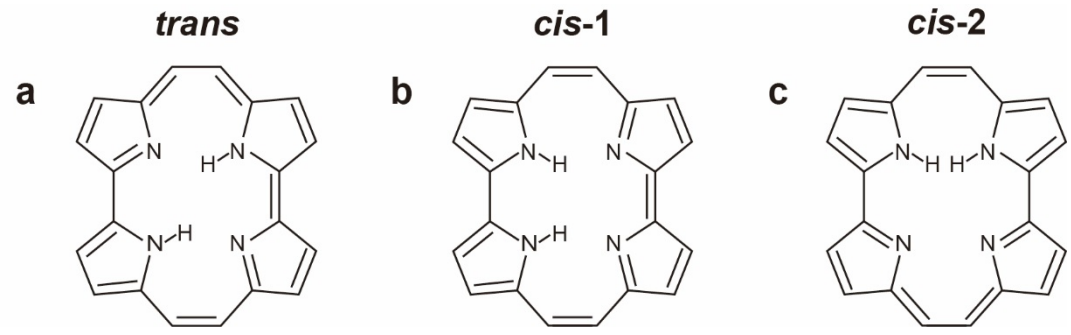

Figure 1 | Different tautomers of porphycene. a, *trans* **b,** *cis*-1 **c,** *cis*-2.

2. Simultaneous STM and AFM imaging

Figure 2 shows simultaneously recorded STM (tunneling current: I_t) and AFM (frequency shift: Δf) images obtained in the constant height mode. In order to record STM images, a small bias voltage (V_{bias}) of ~300 μV was applied to the sample. Such a small bias does not affect Δf signals (see section 6). The gap distance during the measurement was fixed over a Cu(110) surface as follows; first the feedback loop was turned off at the gap resistance of 10 GΩ (I_t = 10 pA with V_{bias} = 100 mV), and then the tip was moved down to the surface by 3.5 Å before scanning.

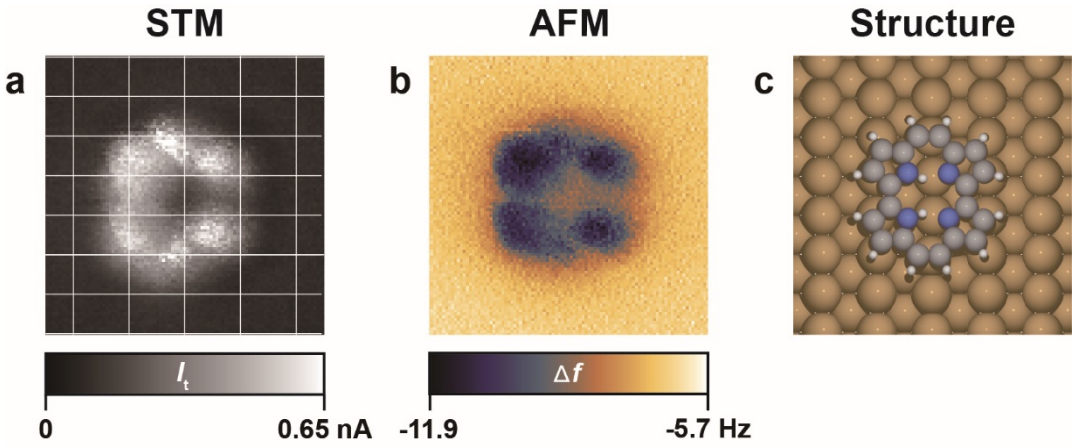

Figure 2 | Simultaneously recorded STM and AFM images. a, STM (I_t) image. The white grid lines represent the surface lattice of Cu(110). **b,** AFM (Δf) image. **c,** Schematics of calculated structure. Measurement parameters: V_{bias} = 300 μV, the oscillation amplitude (A_{osc}) = 3 Å, the resonance frequency (f_0) = 23216.5 Hz, quality factor (Q) = 47468.

3. Effect of a long-range electrostatic force on the tip-induced tautomerization

A contact potential difference (CPD) results in an electrostatic force gradient in the junction that could influence a tip-induced reaction. In order to clarify the effect of this electrostatic force, we examined the tip-induced tautomerization of porphycene under different tip conditions that show a substantially different CPD. The CPD was changed either by applying a pulse voltage or by poking the tip into the surface in a controlled manner. The CPD was evaluated by measuring $\Delta f(V_{bias})$ curves over a Cu(110) surface. **Figure 3a** shows two $\Delta f(\Delta z)$ curves measured under different tip conditions that give significantly different CPDs (see inset). Both $\Delta f(\Delta z)$ curves show very similar features, although the background is considerably different. **Figure 3b** displays several background-subtracted force (F) curves obtained under four different tip conditions, which exhibit different threshold forces and distances. However, there is no clear correlation between the threshold potential (U_{th}) and the CPD (**Fig. 3c**). Therefore, a long-range electrostatic force does not play a crucial role in the tip-induced tautomerization and the observed differences may be due to different atomic structures of the tip apex.

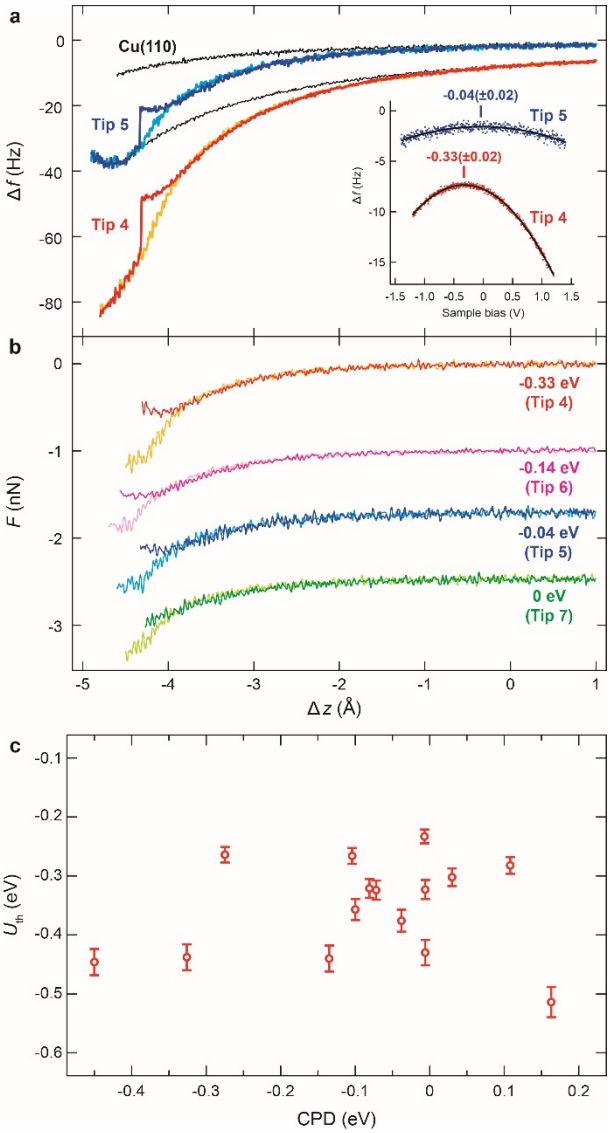

Figure 3 | Force curves measured under tip conditions that gave different CPD. a, Two examples of $\Delta f(\Delta z)$ curves measured for a porphycene molecule and a Cu(110) surface measured under two different tip conditions. The inset shows $\Delta f(V_{bias})$ curves measured over Cu(110) at a gap resistance of 10 GΩ (V_{bias} = 100 mV and I_t = 10 pA). The CPD was determined by fitting the experimental data (dots) to a quadratic function (black solid line). **b,** Series of background-subtracted $F(\Delta z)$ curves. The CPD values are indicated in the figure. The relative tip displacement Δz is with respect to the STM set point of V_{bias} = 100 mV and I_t = 10 pA over Cu(110). Measurement parameters: Tip 4; A_{ocs} = 1 Å, f_0 = 23213.4 Hz, Q = 51714, Tip 5; A_{ocs} = 1 Å, f_0 = 23234.2 Hz, Q = 20315, Tip 6; A_{ocs} = 1 Å, f_0 = 23215.7 Hz, Q = 49610. Tip 7; A_{ocs} = 1 Å, f_0 = 23224.6 Hz, Q = 34051. **c,** Threshold potential as a function of the CPD value. 15 different tips were examined.

4. Reproducibility of the force spectroscopy

Figure 4 shows six approach curves of $\Delta f(\Delta z)$ measured successively over the same porphycene molecule and under the same tip conditions, which demonstrate the reproducibility of force spectroscopy and the tautomerization behavior. The lateral position of the tip was carefully determined by superposing grid lines over the STM image in experiment as shown in the inset to **Fig. 4** (blue lines). Note that the Δf values are substantially different compared to those in **Fig. 2a** of the main text due to different tip conditions. The threshold distance and the Δf value at which tautomerization takes place shows a variation of 0.08 Å and 3.6 Hz, respectively, causing an error of ~100 pN (~60 meV) in the threshold force (potential). This error is most probably due to the small uncertainty of the relative tip position with respect to the molecule.

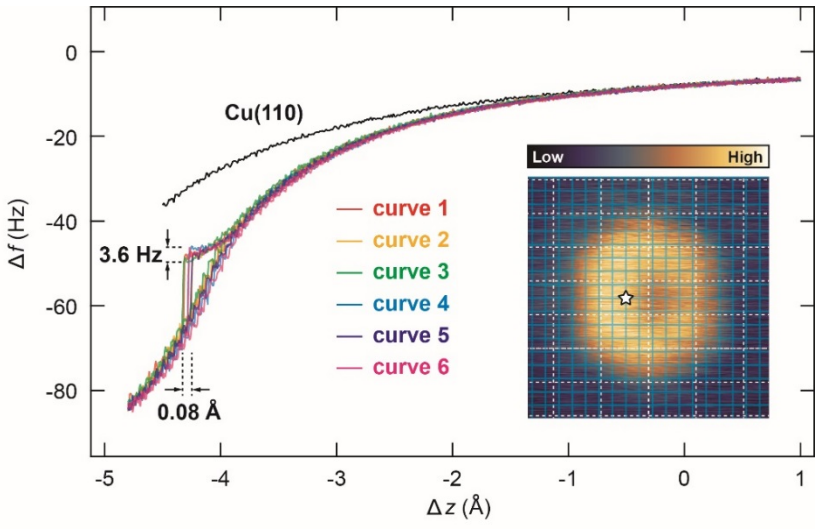

Figure 4 | Six successively-recorded approach curves of frequency shift for a porphycene molecule. The lateral tip position during the measurement is indicated in the STM image (inset). The blue grid lines were superimposed to determine the lateral tip position, while the white dashed lines represent the Cu(110) surface lattice. The black $\Delta f(\Delta z)$ curve was measured over the bare Cu(110) surface. The relative tip displacement Δz is defined with respect to the STM set point of V_{bias} = 100 mV and I_t = 10 pA over Cu(110). Measurement parameters: Tip 4; A_{ocs} = 1 Å, f_0 = 23213.4 Hz, Q = 51714.

5. Tip dependence of the tip-induced tautomerization

Occasionally, a force curve was observed that significantly deviated from the Morse potential model. **Figure 5** displays three typical examples (simultaneously recorded $\Delta f(\Delta z)$ and $I_t(\Delta z)$ curves) that involve a tautomerization event. The deviation appears when the tip approaches the repulsive regime. Then the Δf value decreases again (**Fig. 5a**) or approximates a plateau (**Fig. 5b** and **c**), and $I_t(\Delta z)$ also deviates from an exponential. Tautomerization takes place after this change. Although we recorded the CPD under these tip conditions, any clear correlation between the CPD and the $\Delta f(\Delta z)$ behavior could not be found. Thus the electrostatic force may not be a crucial factor in the observed deviation from the Morse potential model. The deviation might be attributed to a relaxation of the tip apex. Before force spectroscopy measurements, the tip was prepared by the following protocol over a clean Cu(110) terrace; first applying voltage pulse (4–6 V, 50–100 ms) several times, and then poking the tip into the surface (1–2 nm from the STM set point). The force spectroscopy was then carried out if an STM image of a porphycene molecule shows a "good" contrast to determine the lateral tip position. The STM image obtained with Tip 10 (inset of **Fig. 5f**) is an example of a "bad" contrast that was not used for the measurements. We examined 33 different "good" tip conditions, including two different tuning fork sensors, and the significant deviation of $\Delta f(\Delta z)$ curve from the Morse potential model occurred with a probability of ~30 %.

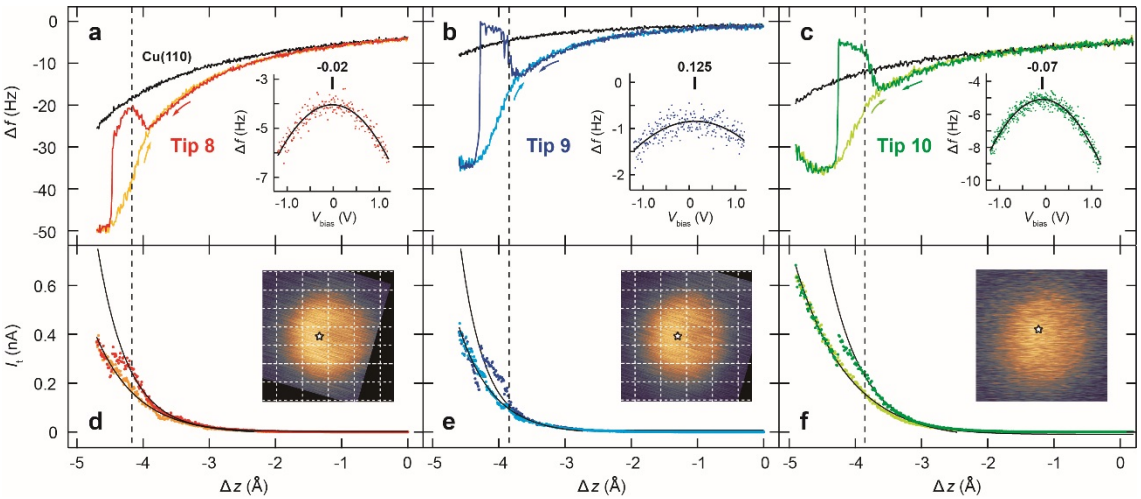

Figure 5 | Examples of frequency shift curves that deviate from the Morse potential model. **a–c,** $\Delta f(\Delta z)$ curves and CPD data measured over Cu(110) at the gap resistance of 10 GΩ (V_{bias} = 100 mV and I_t = 10 pA). **d–f** $I_t(\Delta z)$ curves were simultaneously recorded with $\Delta f(\Delta z)$. The inset shows the STM images obtained under the different tip conditions (2 × 2 nm^2, V_{bias} = 100 mV, I_t = 10 pA). The white dashed lines represent the Cu(110) surface lattice (For Tip 10 this lattice could not be determined due to the blurred image). The relative tip displacement Δz is defined with respect to the STM set point of V_{bias} = 100 mV and I_t = 10 pA over Cu(110). Measurement parameters: Tip 8; $V_{bias} \approx 60$ μV, A_{ocs} = 1 Å, f_0 = 23217.4 Hz, Q = 50264, Tip 9; $V_{bias} \approx 60$ μV, A_{ocs} = 1 Å, f_0 = 23234.2 Hz, Q = 20315, Tip 10; $V_{bias} \approx 150$ μV, A_{ocs} = 1 Å, f_0 = 23217.4 Hz, = 50264.

6. Influence of a small bias voltage and tunneling current on the tip-induced tautomerization

In experiment V_{bias} cannot be exactly zero due to the finite resolution of the instrument, *i.e.*, digital-to-analog convertors (DACs) in Nanonis electronics. A 16-bit resolution of the DACs in our system gives the smallest output resolution of 30 μV in V_{bias} (when the output range of ±1 V is used). Therefore, even if V_{bias} is nominally set to zero, a small tunneling current may flow in the junction due to the unknown offset voltage. The influence of such a small current (and voltage) was found to be negligible from the

experiment in which we carried out the tip-induced tautomerization measurement with a controlled V_{bias} applied. First, $\Delta f(\Delta z)$ curve was carefully examined over a Cu(110) surface in order to verify that the tunneling current has no influence (crosstalk) on the Δf signal. **Figure 6** shows the simultaneously recorded $\Delta f(\Delta z)$ and $I_t(\Delta z)$ curves. V_{bias} is applied to the Cu(110) substrate and the positive and negative values of I_t represent the bias polarity. I_t was collected from the sample to minimize the crosstalk[4]. In **Fig. 6**, it is clear that the Δf signal is fully independent of the current and voltage. Note that the $I_t(\Delta z)$ becomes unstable and is not reproducible when V_{bias} is set to the nominal zero (see inset of **Fig. 6b**). This is presumably due to the random fluctuations of the output voltage.

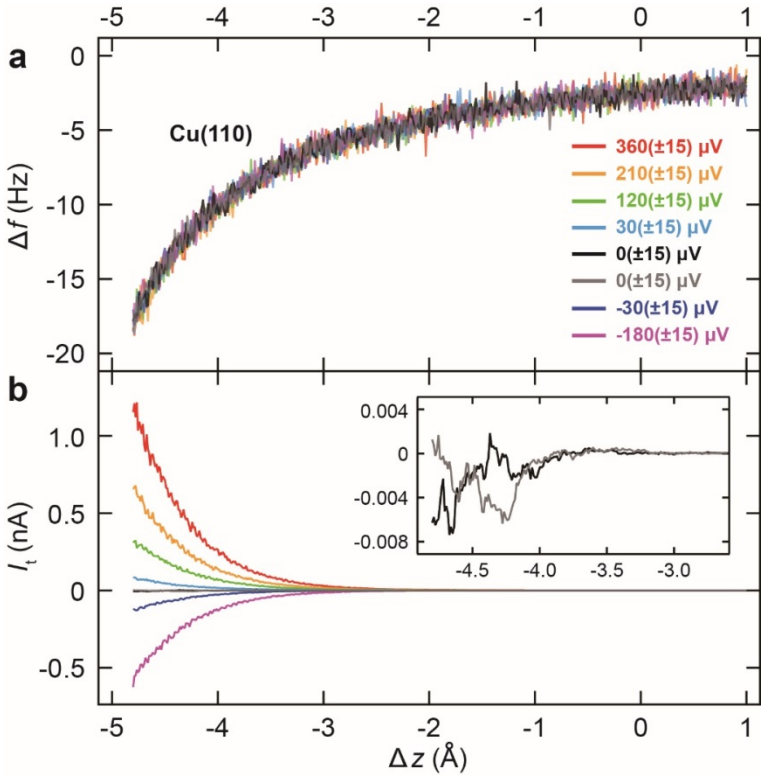

Figure 6 | Simultaneously recorded frequency shift and tunneling current over Cu(110) with a small bias voltage applied. a, $\Delta f(\Delta z)$ curves **b,** $I_t(\Delta z)$ curves. The bias voltages are indicated in **a**. The relative tip displacement Δz is defined with respect to the STM set point of V_{bias} = 100 mV and I_t = 10 pA. The inset in **b** shows the enlarged $I_t(\Delta z)$ curves measured at V_{bias} = 0 V. Measurement parameters: A_{ocs} = 1 Å, f_0 = 23234.2 Hz, Q = 20315.

Next we examined the tip-induced tautomerization with a controlled V_{bias} applied. **Figure 7** displays the simultaneously recorded $\Delta f(\Delta z)$ and $I_t(\Delta z)$ curves for a porphycene molecule. When tautomerization occurs, I_t showed a discontinuous change and the maximum current of 0.16, 0.25, and 0.35 nA was observed for 30(±15), 60(±15), 90(±15) μV, respectively, just before this event. However, the threshold Δf and Δz are essentially the same for the three cases, clearly indicating a negligible effect of small current and voltage on the tip-induced tautomerization.

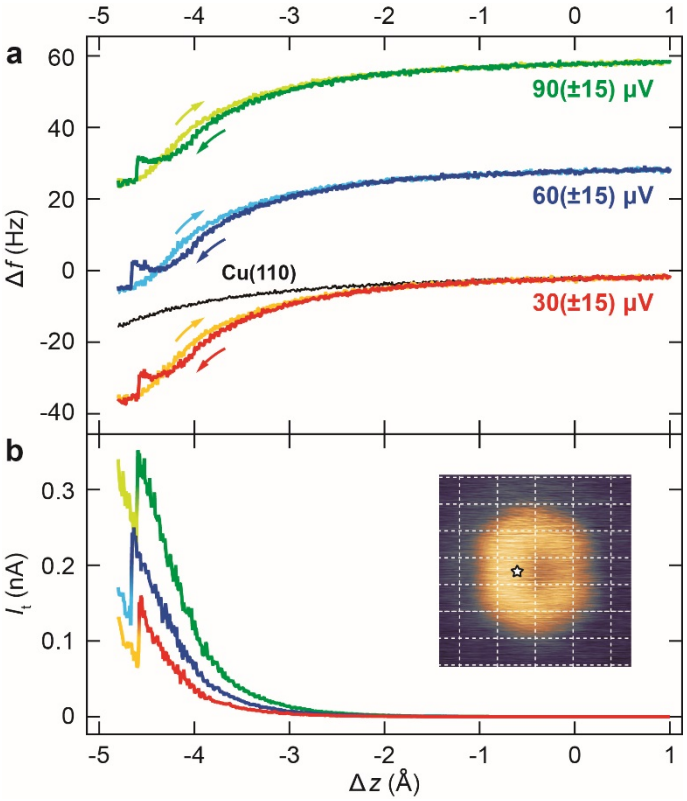

Figure 7 | Simultaneously recorded frequency shift and tunneling current over a porphycene molecule with a small bias voltage applied. a, $\Delta f(\Delta z)$ curve. The bias voltages used are indicated in the figure. $\Delta f(\Delta z)$ curves for V_{bias} = 60 μV and 90 μV are vertically displaced for clarity. **b,** $I_t(\Delta z)$ curve during approach. The lateral tip position during measurement is indicated by a star in the inset STM images. The relative tip displacement Δz is defined with respect to the STM set point of V_{bias} = 100 mV and I_t = 10 pA over Cu(110). Measurement parameters: Tip 4; A_{ocs} = 1 Å, f_0 = 23213.4 Hz, Q = 51714.

7. Distribution of the threshold distance of the tip-induced tautomerization

Figure 8 shows the distribution of the threshold distance (Δz_{th}) at which a tautomerization event takes place, measured with different tip conditions. In **Fig. 8a** and **b**, Δz_{th} is defined with respect to the equilibrium distance (z_e, *i.e.*, potential minimum) of the approach curve and to the STM set point of V_{bias} = 100 mV and I_t = 10 pA over Cu(110), respectively. In either case Δz_{th} shows a comparable distribution (0.6–0.7 Å). It is clear from **Fig. 8a** that tautomerization takes place near the potential minimum.

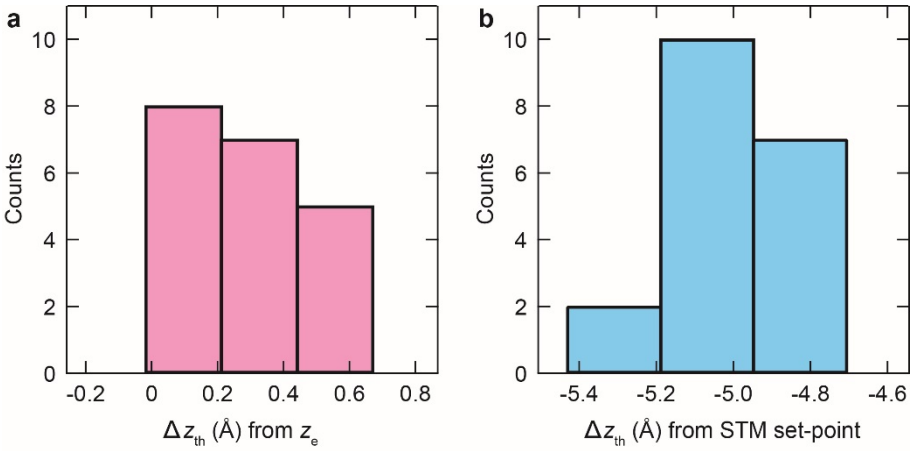

Figure 8 | Threshold distance for the tip-induced tautomerization. Distribution of Δz_{th} defined with respect to z_e **a** and the STM set point **b**.

8. Tip-induced *cis* → *trans* tautomerization

In most cases, the *cis* → *cis* conversion of porphycene was observed in the tip-induced tautomerization. However, the *cis* → *trans* conversion rarely occurred (depending on the tip conditions). **Figure 9a** and **b** shows the STM images before and after the measurement in **Fig. 9c**. In $\Delta f(\Delta z)$ curve, a discrete change occurs in the retraction, and then the Δf signal shows fluctuations until around the turning point. After the

measurement, the STM image of porphycene becomes symmetric that looks very similar to the *trans* configuration observed on a Cu(111) surface[3]. The STM appearance of the *trans* molecule also suggests that the molecular orientation would be different from the *cis* form and it appears to be rotated.

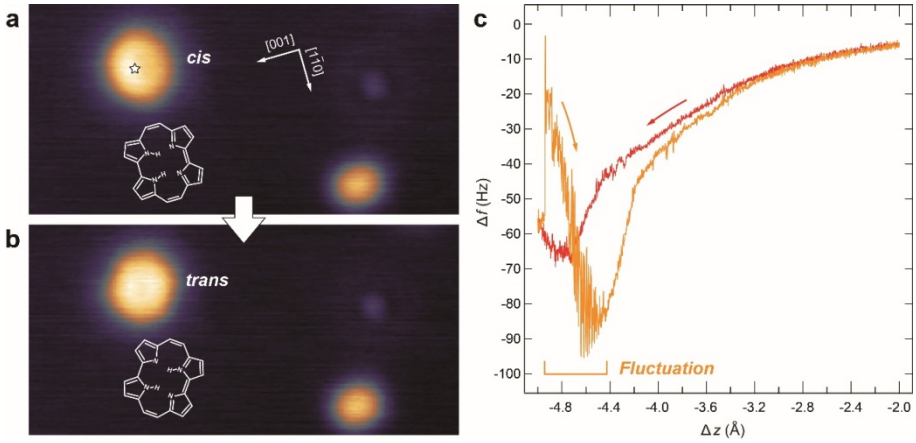

Figure 9 | Tip-induced *cis* → *trans* tautomerization. a and **b,** STM images of porphycene before (*cis*) and after (*trans*) the force curve measurement. **c,** $\Delta f(\Delta z)$ curve obtained at the white star position in **a**. A discrete change of the Δf occurs in the retraction (orange curve) followed by a fluctuating (unstable) Δf signal. The relative tip displacement Δz is defined with respect to the STM set point of V_{bias} = 100 mV and I_t = 10 pA over Cu(110) surface. Measurement parameters: A_{ocs} = 0.5 Å, f_0 = 22640.5 Hz, Q = 60013.

9. Position adjustment of the force map

It is not a trivial task to accurately adjust the experimental force map to the calculated structure. We implemented this using the following protocol. In experiment the lateral tip position was determined by superposing the grid lines on images (as shown in the inset of **Fig. 4**). The lateral tip position can be estimated with respect to the porphycene molecule by comparing to the underlying Cu(110) surface lattice. Assuming that the short-range tip–molecule interaction is determined by the foremost atom on the tip, each

force curves measured over the acceptor pyrrole side (blue filled circles in **Fig. 10a**) should be identical with the spectra at the corresponding position after tautomerization (red open circles in **Fig. 10b**). **Figure 10c** shows a series of the recorded spectra that were carefully compared to give the most consistent result; after tautomerization $\Delta f(\Delta z)$ curve over the donor pyrrole side should be the same with the corresponding counterpart over the acceptor pyrrole side. The slight deviations between them may be due to experimental uncertainties in determining the precise lateral and vertical tip position (see **Fig. 4**) and/or due to an asymmetric geometry of the tip apex. However, we believe that this protocol gives an accuracy of ±0.4 Å in the lateral tip position.

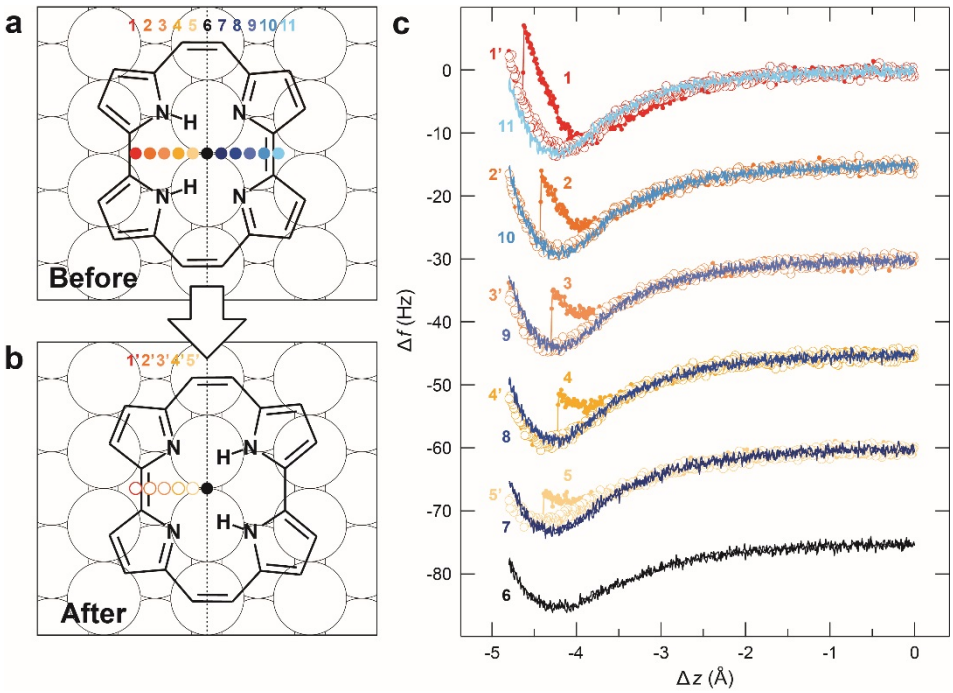

Figure 10 | Position adjustment of force map. a and **b,** Schematics of the calculated structures before and after tip-induced tautomerization. The lateral tip positions during the force curve measurements are indicated by the colored markers **c**, Approach and retraction $\Delta f(\Delta z)$ curves over a porphycene molecule. The tautomerization is induced exclusively over the donor pyrrole sides (red filled circles in **a**) and the backward spectra (open red circles in **b**) are compared to those measured over the acceptor pyrrole side (filled blue circles in **a**). The relative tip displacement Δz is defined with respect to the STM set point of V_{bias} = 100 mV and I_t = 10 pA over Cu(110). Measurement parameters: A_{ocs} = 1 Å, f_0 = 22646 Hz, Q = 39143.

10. Force mapping with a different tip

Figure 11a shows the force map obtained under different tip conditions (Tip 3 in **Fig. 2b** of the main text). Although the maximal attractive force is larger than that in **Fig. 2f** of the main text, the map shows consistent features.

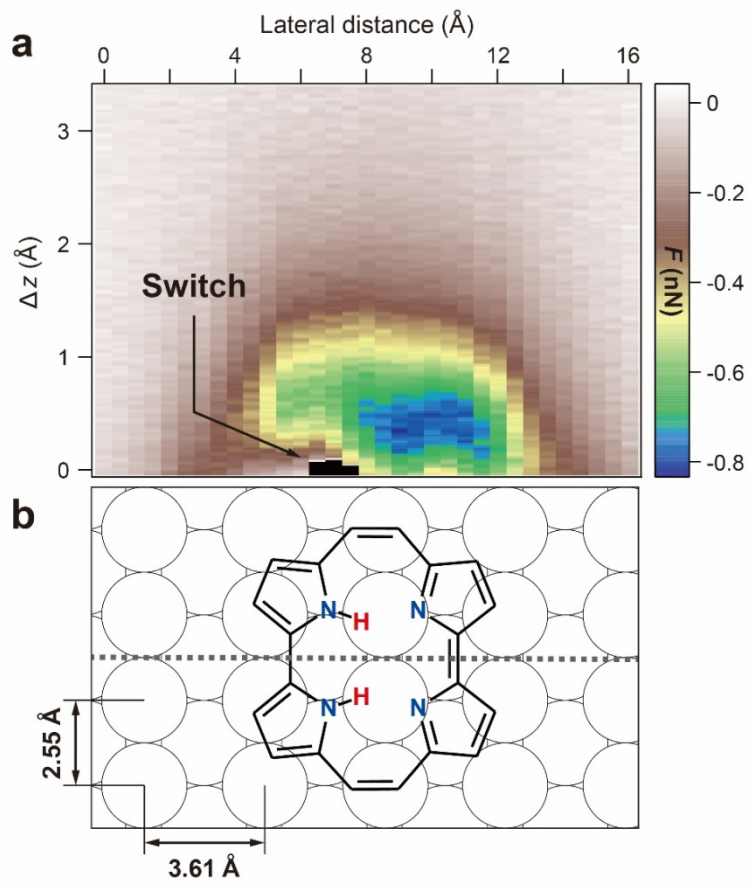

Figure 11 | Force map over a porphycene molecule obtained with Tip 3. The Δz represents the tip height with respect to z_e at position (ii) in **Fig. 2g** of the main text. Measurement parameters: A_{ocs} = 1 Å, f_0 = 22646 Hz, Q = 39143.

11. Fitting parameters for the force curves

Table 1 Fitting parameters used for **Fig. 2b** of the main text.

	Forward (approach)		Backward (retraction)	
	E_d (eV)	κ (Å^{-1})	E_d (eV)	κ (Å^{-1})
Tip 1	0.272 (0.003)	1.33 (0.02)	0.444 (0.003)	1.30 (0.01)
Tip 2	0.463 (0.004)	1.22 (0.05)	0.678 (0.01)	1.23 (0.01)
Tip 3	0.599 (0.003)	1.27 (0.01)	0.720 (0.003)	1.34 (0.01)

12. Computational methods

The total energy, geometries, minimum energy paths (MEPs) and vibrational modes and frequencies of the adsorbed porphycene molecule were determined from periodic, plane-wave density functional theory (DFT) calculations using the Vienna ab-initio simulation program (VASP) [5]. The electron-ion core interactions and the exchange-correlation effects were treated using the Projector Augmented Wave (PAW) method[6] and the optB86B version of the van der Waals density functional[7, 8, 9, 10] respectively. The plane-wave cut-off was 400 eV. The Cu(110) surface was represented in a super-cell by a four layer slab with a 4×6 surface unit cell and a 20 Å vacuum region. The tip was modelled by a pyramid of five Cu atoms and the Xe terminated tip was modelled by a Xe atom adsorbed on the Cu apex atom of the pyramid. A 2×2×1 grid was used in the *k*-point sampling. The structures were relaxed until all forces were less than 0.01 eV/Å, with the bottom two Cu layers kept fixed throughout the geometry optimization at the calculated lattice constant of 3.60 Å. The supercell size was kept fixed for the different structures explored. The vibrational spectrum of the adsorbed molecule on a rigid substrate lattice was calculated by diagonalising the dynamical

matrix which was obtained by finite differences of the calculated forces at symmetric ionic displacements of 0.02 Å. The MEPs and the reaction barriers were calculated using the nudged elastic band (NEB) method[11, 12].

13. Calculated force curve

The total energy for the combined surface–porphycene–tip system was calculated as a function of the relative displacement (Δz) of the Cu_5 cluster to the surface. An example of simulated potential energy curves over the molecule and Cu(110) are shown in **Fig. 12**. Here the lateral tip position is fixed at Δx = -1.8 Å over the molecule. The background-subtracted potential energy $U(\Delta z)$ over the molecule was obtained from the difference between potential energies over the molecule and Cu(110) and imposing U = 0 at Δz = 6.7 Å. The corresponding background-subtracted tip-surface force, $F(\Delta z) = -\frac{dU}{dz}(z)$, was obtained by numerical differentiation. The 2D plots, shown in **Fig. 4** of the main text and **Fig. 13**, were obtained by interpolating a series of background-subtracted curves at different lateral positions of the tip.

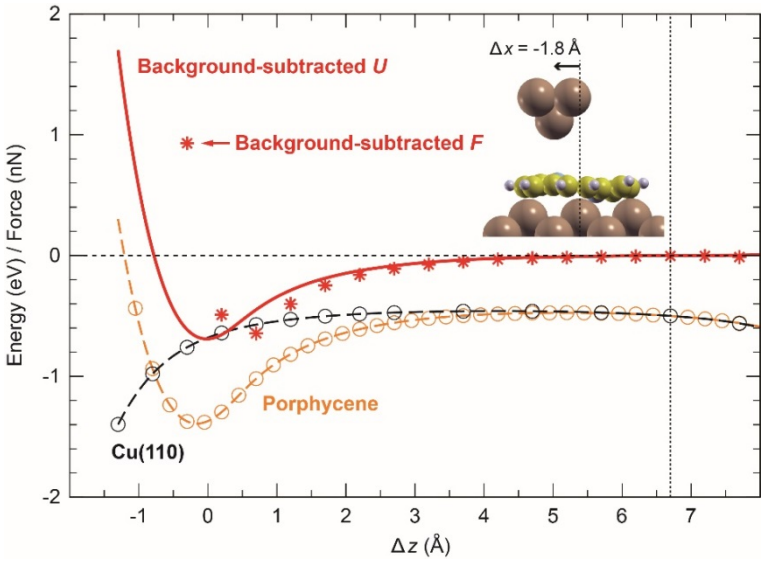

Figure 12 | Calculated total energy and force curves. The Cu_5 tip approach to the Cu(110) surface with or without the adsorbed porphycene molecule. The lateral tip position was is fixed at Δx = -1.8 Å over the molecule. The solid red line and the red symbols represent the background-subtracted $U(\Delta z)$ and $F(\Delta z)$, respectively. The relative displacement Δz is defined with respect to the energy minimum of background-subtracted $U(\Delta z)$.

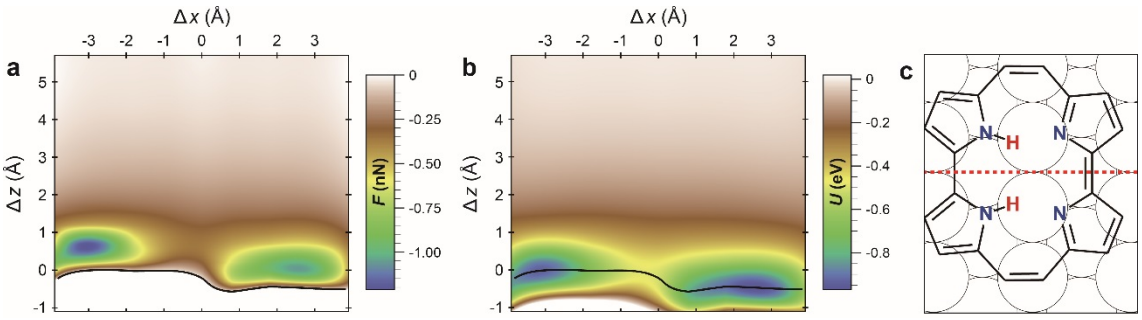

Figure 13 | Contour plots of calculated background-subtracted force and potential map. a, $F(\Delta x, \Delta z)$. **b,** Potential $U(\Delta x, \Delta z)$. The black line in **a** and **b** indicates the contour of $F = 0$. **c,** Schematic of the adsorption structure. The red line represents the vertical plane of the map. The relative displacement Δz is defined with respect to the energy minimum of background-subtracted $U(\Delta z)$ at Δx = -1.8 Å.

14. Minimum energy paths for step-wise and concerted tautomerization

The calculated MEPs for the tautomerization of porphycene between the initial and the final mirror reflected *cis* configurations predict that the step-wise mechanism is clearly favored over the concerted mechanism. The MEP for the step-wise mechanism (**Fig. 4f** of the main text) was obtained by constraining the path to pass through one of the two intermediate, degenerate *trans* configurations, whereas the concerted path was obtained by enforcing reflection symmetry through the vertical mirror plane of the adsorbed molecule in the *cis* configurations.

As shown in **Fig. 4f** of the main text, the step-wise path is symmetric with respect to the *trans* configuration and has a potential energy barrier of 342 and 168 meV for the *cis* → *trans* and the *trans* → *cis* transitions, respectively. In order to compare these barriers with experiments, one needs at least to correct for the large zero-point energies (ZPE) of the two inner H atoms. The corrected energies for the stable configurations and the transition states are given by,

$$U_C(X) = U(X) + U_{\mathrm{ZPE}}(X) - U_{\mathrm{ZPE}}(X = cis_i), \qquad (1)$$

where $U(X)$ and $U_{\mathrm{ZPE}}(X)$ is the potential and the ZPE, respectively, of the configuration X and cis_i is the initial *cis* configuration. Here the ZPE were obtained from the calculated vibrational energies of the two inner H atoms, when only these two atoms were allowed to move. At the barrier configuration, one of the modes is unstable, which shows that this configuration is indeed a transition state. The resulting ZPE corrections reduce the energy barriers to 203 and 19 meV for the *cis* → *trans* and the *trans* → *cis* transitions, respectively. Note that the ZPE reduction of the energy barrier of about 140 meV is close to the value of about 170 meV for the ZPE of the N–H stretch. Furthermore, the relatively large path length between the initial and final configuration

indicates that there are substantial movements of not just the inner H atoms during the tautomerization.

As shown in **Fig. 14**, the concerted path is also symmetric with respect to the initial and final *cis* configurations but exhibits only a single potential energy barrier with a height of 628 meV, which is much larger than the barriers for the step-wise path. The ZPE corrections reduces this energy barrier to 352 meV, which is still significantly larger than that of the step-wise path. Furthermore, the barrier configuration has two unstable modes and is therefore not a first order saddle point and a proper transition state.

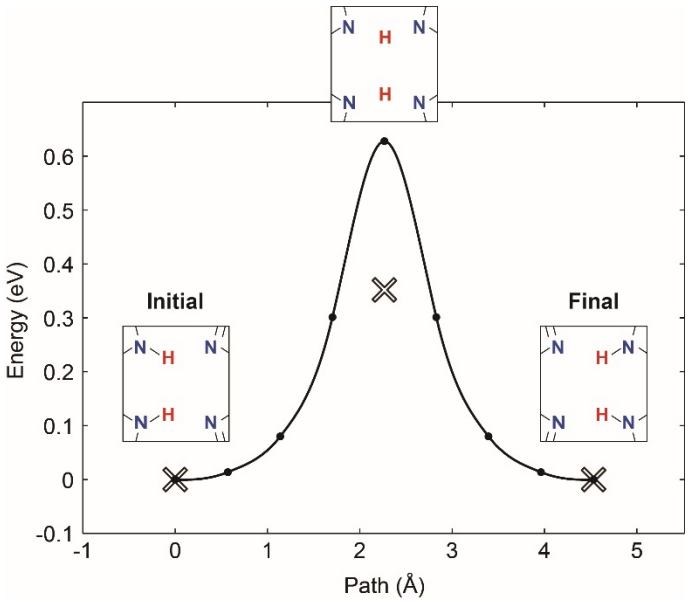

Figure 14 | Concerted tautomerization path for the *cis* → *cis* configurations in the absence of a tip. As in **Fig. 4f** of the main text, the solid line is obtained by an interpolation to the calculated energies of the images (solid circles) in the NEB calculations and their tangential forces along the path, which are not shown. The ZPE corrected energies are indicated by crosses. The path length was obtained from the Euclidean distance between the images in configurations space.

15. Red-shift of the N–H stretching mode frequency

The frequency of the N–H stretching mode exhibits a red-shift, *i.e.*, a softening of the N–H bond, when the tip approaches a porphycene molecule. **Figure 15a** shows the dI/dV spectrum measured over a molecule with the tip fixed at the same position as in the force spectroscopy, *e.g.*, in **Fig. 2a–c** of the main text. The dI/dV spectrum shows a characteristic dip at the energy of the N–H stretching excitation[13]. **Figure 15b** displays the two-dimensional plot of the dI/dV spectra measured at different tip heights defined by I_t. It is clear that the dip position shifts to lower voltages (energies) at smaller tip–molecule distances. This red shift of the vibrational frequency suggests weakening of the N–H bond strength and strengthening of H bonds within the molecular cavity, thus the change in the N–H···N geometry that is directly associated with the tautomerization coordinate. This change could cause the reduction of the tautomerization barrier. Note that the dI/dV spectra were measured with the pure STM configuration (not qPlus sensor) in order to obtain better signal-to-noise ratio. It should be noted that due to the absence of the oscillation, the tip height at a given set point defined by tunneling conditions is different from the one in the qPlus configuration and the tip is expected to be closer to the surface approximately as much as an A_{OSC}. **Figure 15c** shows the calculated N–H harmonic vibrational energies as a function of the tip–molecule distance. For simplicity only a single H-atom in the cavity is considered free to move. The red-shift of the frequency is predicted around the potential minimum (from 0.5 to -0.5 Å) where elongation of the N–H bond also takes place (**Fig. 4g** of the main text).

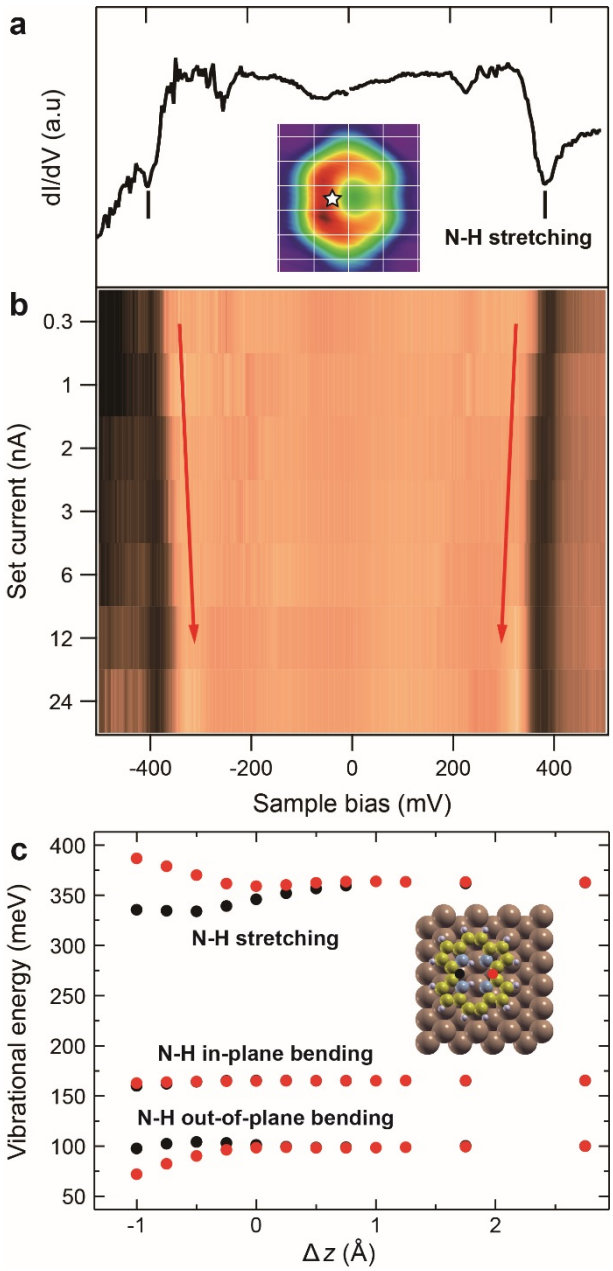

Figure 15 | Red-shift of the N–H stretching mode. a, dI/dV spectrum measured over a porphycene molecule. **b,** dI/dV spectra measured at different tip heights given by V_{bias} = 0.1 V and the tunneling current indicated on the vertical axis. The lateral tip position during the measurement is indicated by the white star in the STM image shown in the inset. **c,** Calculated harmonic vibrational energies of N–H modes as a function of Δz and for two different lateral tip positions. The tip position is indicated by the red and black dots in the schematic structure shown in the inset. The relative displacement Δz is defined with respect to the energy minimum of the background-subtracted $U(\Delta z)$ at Δx = -1.8 Å (see **Fig. 12**).

16. Relaxation of Xe-terminated tip

The simulations with a Xe-terminated tip was carried out by extending our Cu_5 cluster with a Xe atom at the tip apex, as shown in **Fig. 16a**. The background-subtracted potential energy curves $U(\Delta z)$ and the corresponding force curves $F(\Delta z)$ are shown in **Fig. 16b**. We find that the interaction energy between the adsorbed molecule and the physisorbed Xe atom on the tip is generally much weaker than for the Cu_5 tip. Also the repulsive regime is much softer due to a strong bending of the Xe atom near and in contact with the molecule (**Fig. 16c** and **d**). This suggests that a Xe tip is too soft and chemically inert to exert the forces necessary to induce tautomerization.

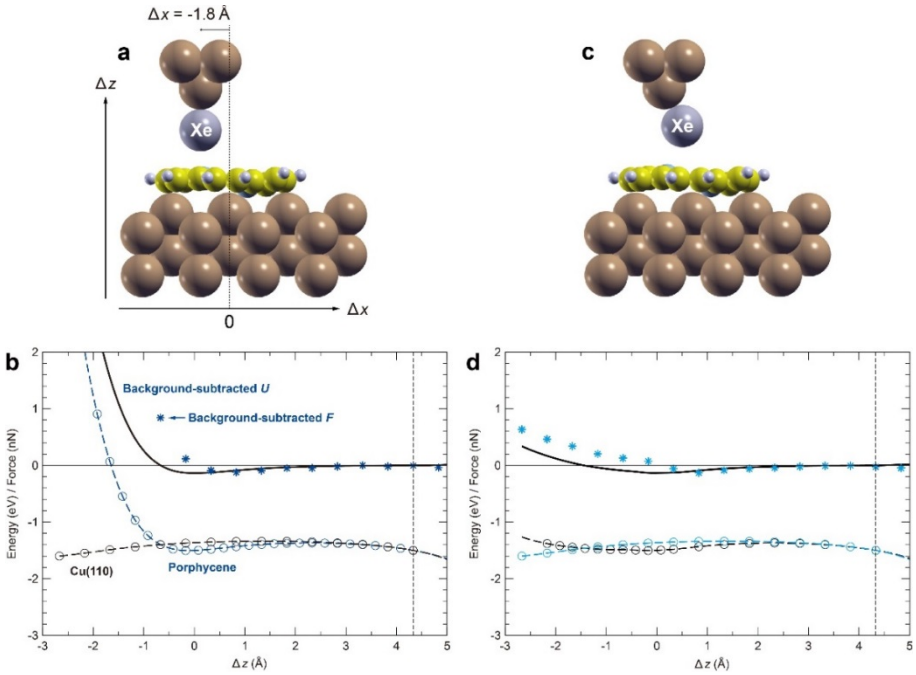

Figure 16 | Model of the Xe-tip approach to adsorbed porphycene on Cu(110). a, Snapshots of the structure during approach of a frozen Xe-tip. **b,** Force (potential) curve with a frozen Xe-tip. **c,** Snapshots of the structure during approach of a relaxed Xe atom on the frozen Cu_5 cluster. **d,** Force (potential) curve with a relaxed Xe atom on the tip. The lateral tip position over the molecule is fixed at Δx = -1.8 Å. The background-subtracted potential energy curve $U(\Delta z)$ (black line) is obtained as the energy difference between the total energies with and without the adsorbed molecule and by imposing $U = 0$ at Δz = 4.3 Å. The relative displacement Δz is defined with respect to the energy minimum of $U(\Delta z)$ with a frozen Xe-tip. Note that when the Xe atom is relaxed, Δz characterizes the relative movement of the rigid Cu-cluster.

17. Minimum energy paths for tautomerization in the presence of a Xe-terminated tip.

Figure 17 shows the calculated MEPs with the Xe-tip for the step-wise mechanism (*cis* → *trans* → *cis*). The overall energy barrier is calculated to be 0.72 and 1.07 eV for Δz = -0.7 and -1.7 Å, respectively, and the corresponding ΔU is 101 and 22 meV. It should be noted that the reaction barrier and length are both significantly larger than those of the Cu_5 tip (**Fig. 4h** of the main text). This difference is due to the Xe atom being in the way for the reaction resulting in large motions of the Xe atoms and the atoms in the molecule in the reaction path.

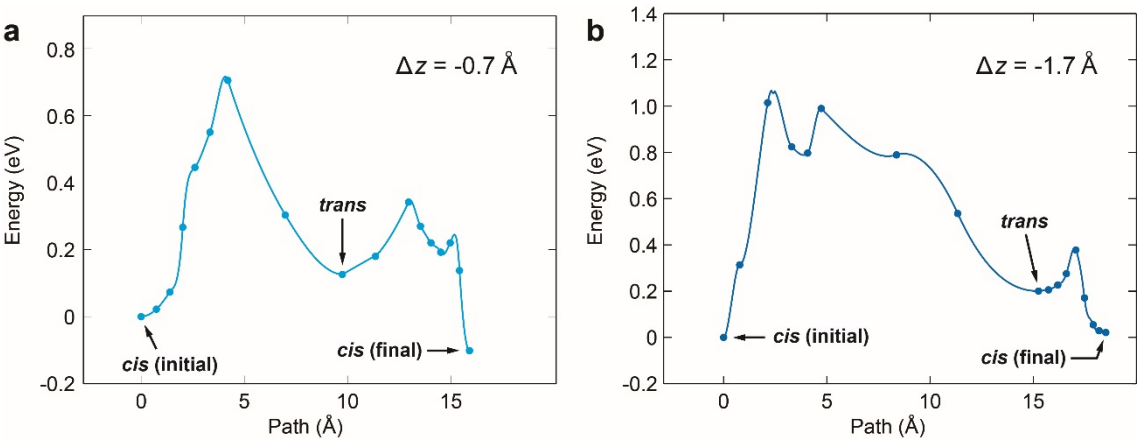

Figure 17 | Tautomerization paths in the presence of a Xe-terminated tip. Calculated MEPs between the initial and final *cis* configurations for **a,** Δz = -0.7 Å **b,** -1.7 Å. Lateral tip position and definition of Δz as in **Fig. 16**. The interpolation between the calculated images and the path length were obtained as in **Fig. 14**.

References

[1] Wu, Y.-D. *et al.*, Porphyrin Isomers: Geometry, Tautomerism, Geometrical Isomerism, and Stability. *J. Org. Chem.* **62**, 9240–9250 (1997).

[2] Kumagai, T. *et al.* Controlling intramolecular hydrogen transfer in a porphycene molecule with single atoms or molecules located nearby. *Nature Chemistry* **6,** 41–46 (2014).

[3] Ladenthin, J. N. *et al.* Hot Carrier-Induced Tautomerization within a Single Porphycene Molecule on Cu(111). *ACS Nano* **9,** 7287–7295 (2015).

[4] Majzik, Z. *et al.* Simultaneous current, force and dissipation measurements on the Si(111) 7×7 surface with an optimized qPlus AFM/STM technique. *Beilstein J. Nanotechnol.* **3**, 249–259 (2012).

[5] Kresse, G. & Furthmüller, J. Efficient iterative schemes for ab initio total-energy calculations using a plane-wave basis set. *Phys. Rev.* B **54**, 11169 (1996).

[6] Kresse, G. & Joubert, D. From ultrasoft pseudopotentials to the projector augmented-wave method. *Phys. Rev.* B **59**, 1758 (1999).

[7] Dion, M., Rydberg, H., Schröder, E., Langreth, D. C. & Lundqvist, B. I. Van der Waals Density Functional for General Geometries. *Phys. Rev. Lett.* **92**, 246401 (2004).

[8] Román-Pérez, G. & Soler, J. M. Efficient Implementation of a van der Waals Density Functional: Application to Double-Wall Carbon Nanotubes. *Phys. Rev. Lett.* **103**, 096102 (2009).

[9] Klimeš, J., Bowler, D. R. & Michaelides, A. Chemical accuracy for the van der Waals density functional. *J. Phys. Cond. Matt.* **22**, 022201 (2010).

[10] Klimeš, J., Bowler, D. R. & Michaelides, A. Van der Waals density functionals applied to solids. *Phys. Rev.* B **83**, 195131 (2011).

[11] Mills, G., Jónsson, H. & Schenter, G. K. Reversible work transition state theory: application to dissociative adsorption of hydrogen. *Surf. Sci.* **324**, 305–337 (1995).

[12] Henkelman, G., Uberuaga & B. P., Jónsson, H. A climbing image nudged elastic band method for finding saddle points and minimum energy paths. *J. Chem. Phys.* **113**, 9901–9904 (2000).

[13] Kumagai, T. *et al.* Thermally and Vibrationally Induced Tautomerization of Single Porphycene Molecules on a Cu(110) Surface. *Phys. Rev. Lett* **111,** 246101 (2013).